Unraveling the spatial distribution of the acidity of HZSM-5 zeolite on the level of crystal grains

Xiaochao Xian[1*], Jun Chen[1], Yirong Chu[1], Mengjun He[1], Shuo Zhao[1*], Lichun Dong[1] and Jingzheng Ren[2]

[1]School of chemistry and chemical engineering, Chongqing University, No.174 Shazhengjie, shapingba, Chongqing, 400044, China

[2]Department of Industrial and Systems Engineering, The Hong Kong Polytechnic University, Hong Kong, China

ABSTRACT

Here we developed a new method to quantitatively characterize the spatial distribution of the Brønsted acidity of HZSM-5 zeolite on the crystal grains level indirectly. The Brønsted acid sites of HZSM-5 zeolite completely covered or blocked by previous coke deposition were released gradually from the outer surface to the center of the crystal grains via shrinking core mode isothermal oxidation with high temperature and low oxygen concentration. The spatial distribution of the coke was obtained based on the one-dimensional position coordinate L_{rp} through building and solving an enhanced shrinking core model (ESCM). Then the released acidity characterized by *n*-propylamine temperature-programmed decomposition was correlated to the specific position of L_{rp}. The results show that the acid density is roughly homogenous while the acid strength is heterogeneous within the crystal grains. From the outer surface to the center of the crystal grains, the strength of the Brønsted acid sites increase gradually.

* Corresponding author: Xiaochao Xian, Email: xianxch@cqu.edu.cn
Shuo Zhao, Email: zhaoshuo@cqu.edu.cn

Topical Heading: Reactors, kinetics, and catalysis

Keywords: acidity, HZSM-5 zeolite, spatial distribution, coke deposition, isothermal oxidation

INTRODUCTION

As a typical shape-selective catalyst, HZSM-5 zeolite has been widely used in several important process such as petrochemical process[1,2], methanol-to-olefins (MTO)[3-7], methanol to hydrocarbons[8-10], supercritical catalytic cracking[11-15], etc. Brønsted acid sites stemming from the presence of protons balancing the negative charge induced by the framework Al atoms in tetrahedral sites (T-sites) provide the primary intrinsic catalytic activity for HZSM-5 zeolite. Effective characterization of the acidic properties is critical to the rational design and preparation of individual HZSM-5 zeolites for specific applications.

The acidity of zeolite catalysts is generally characterized by bulk methods such as NH_3-TPD, FTIR and pyridine-FTIR[16], which provides the statistical average information on the nature, density and strength of the acid sites. However, the importance of the spatial distribution of the acid sites in HZSM-5 zeolite catalyst is gaining increasing attention due to the requirement of rational catalyst design[17]. The effects of the spatial distribution of the acidity on the reactivity of HZSM-5 zeolite can be understood from two aspects. First, the variation on the crystallographic distribution of the T-sites results in heterogeneous chemical environment or intrinsic activity of the acid sites[18-20]. Second, the accessibility of the reactant molecules to the acid sites, steric constraint of the transition state geometry or the difficulty of the diffusion of the products is affected by the locations of the acid sites either from the perspective of channel system or crystal particle[21-25].

Several new methods have been developed to locate the acid sites on different levels. On the level of crystal unit cell, the challenging Al siting (*i.e.*, location of the T-sites) can now be partially analyzed by the combination of ^{27}Al 3Q MAS NMR spectroscopy and computational chemistry methods (including QM/MM or DFT/MM)[18,26] or MD-EXAFS method[27]. On the level of channel system, the approximate identification of the acid sites in the channel intersections (*ca.* 0.9 nm) from those in the straight channels (0.53×0.56 nm) or sinusoidal channels (0.51×0.55 nm) has also been investigated by the combination of ^{27}Al MAS NMR with the features of some well-known probe reactions (*e.g.*, constraint index (CI) or Co(II) ion UV-vis DRS)[6,23,28-32]. The potential interactions of different acid sites might also affect the acidic properties of individual acid sites. The short-range effect stemming from spatial proximity of adjacent Brønsted acid sites has been investigated by ^{1}H double quantum (DQ) MAS NMR, ^{13}C MAS NMR, Co(II) ion UV-vis DRS or computational chemistry method[33-35]. Although less mentioned, the long-range interaction of different acid sites has also been primarily revealed by ^{1}H MAS NMR[36,37]. In common, the above mentioned investigations on the spatial distribution of acid sites is predominately based on the characterization of the local chemical environment of individual acid sites.

On the level of crystal grains (in the scale of micron or sub-micron according to the specific crystal size), however, the understanding of the acid distribution is quite limited due to the lack of effective methods. Obviously, the local chemical environment characterization methods are ineffective. The theoretical calculation methods are also invalid due to both the insufficient computational ability to explore such a macro-system (*i.e.*, a crystal grain) containing more than millions of unit cells and the difficulty in constructing a crystal model

with rigorously consistent structure with that of a real zeolite[17,19]. Under this background, the *in situ* monitoring of the probing reaction by fluorescence microscopy has been developed to map the spatial distribution of active sites in heterogeneous catalysts on the level of single catalyst particle or crystal particle[38,39]. By using the stochastically occurred reaction of single probe molecule, *i.e.*, single-molecule fluorescence microscopy (SFM), the spatial resolution of fluorescence microscopy has been enhanced from 250 nm (the diffraction limit) down to *ca*. 10 ~ 20 nm[40-42]. The SFM method has been applied to map the activity of the acid sites in ZSM-22 and ZSM-5 zeolite, the results revealed that the spatial distribution of catalytic activities in either ZSM-22 nanorod or ZSM-5 crystal particle is nonuniform due to the existence of edge and defects even in a seemingly perfect crystal[40,42]. The correlated ultrastructure-reactivity information obtained by integration of transmission electron and single-molecule fluorescence microscopy (SFM-TEM) confirmed the existence of intrinsic differences in reactivity of the acid sites in different HZSM-5 crystal particles or even within the same zeolite crystal particle[43]. Very recently, a tip-enhanced fluorescence microscopy (TEFL) method was developed to provide direct two-dimensional hyperspectral information (without the complex post process of data required in SFM), and the results also recognized the nonuniform spatial distribution of Brønsted acidity within individual zeolite crystals[44]. Therefore, the investigation of acid distribution on the level of crystal grains is necessary and valuable.

However, the above mentioned methods based on SFM still have limitations on both the quantitative and the qualitative characterization of the spatial distribution of acid sites of HZSM-5 zeolite on the level of single crystal particle. First, the microscopic method only

provides local information in a specific catalyst particle, which might not represent the global acid property of a lot of catalyst particles used in actual catalytic reaction. Second, although the spatial resolution has been enhanced to *ca*. 10 nm within the two-dimensional plane, actually the observed image is the overlapped results on the vertical direction of the "thin section" with a thickness ≥ 100 nm (*ca*. 100 nm for the actual section prepared by FIB or 200~300 nm for virtual section of focal plane), *i.e.*, the resolution in the 3-dimensional space is still limited. Third, neither the absolute acid density nor acid strength of individual acid sites can be provided quantitatively.

In this work, in order to characterize the spatial distribution of acid sites of HZSM-5 zeolite on the level of crystal grains, we proposed a new idea based on the knowledge of chemical reaction engineering to map the acidity of HZSM-5 zeolite from the outer surface to the center of the crystal grains. Through the manipulation of coke deposition and shrinking core mode oxidation, the acid sites at different positions along the *one-dimensional coordinate* (L_{rp}) were previously masked and then released as designed. The density and the strength of the released Brønsted acid sites were first characterized by the *n*-propylamine temperature-programmed decomposition (*n*-propylamine TPD) method[45,46], and then quantitatively correlated to L_{rp}, which was obtained by solving an enhanced shrinking core model (ESCM) accounting for the coke oxidation process.

EXPERIMENTAL

Preparation of coked HZSM-5 zeolite

Particle HZSM-5 zeolite catalyst (20-40 mesh) was prepared from pure HZSM-5 zeolite powder (SiO_2/Al_2O_3 = 50, Nankai University Catalyst Co.,Ltd.) without any binder or matrix.

The coke deposition was achieved through the supercritical catalytic cracking of *n*-dodecane at 500℃ and 4.0 MPa for 4 h. In a typical run, 1.000 g HZSM-5 catalyst particles were loaded in a fixed-bed reactor[13]. After the pressure and temperature had been raised to the set points by compressed nitrogen and electoral heating, respectively, the catalyst was activated at 500℃ for 1 h with flowing nitrogen (200 cm^3/min). Then liquid *n*-dodecane reactant was fed into the reactor by a high pressure liquid chromatography pump (SSI-I series) with a flow rate of 1.00 cm^3/min at room temperature. The evolution of the conversion of *n*-dodecane was tracked by the analysis of the liquid product samples through gas chromatography analysis using *n*-tridecane as internal standard substance. When the time on stream reached 4 h, the reaction was terminated by stopping feeding, turning off heating and releasing pressure sequentially. The catalyst bed was purge by nitrogen (500 cm^3/min for 15 min and then reduced to 200 cm^3/min) to remove the trapped or adsorbed species until cooled down to room temperature. The coked HZSM-5 zeolite catalyst prepared by several individual runs was mixed together for the following investigations of coke oxidation and acidity or other characterizations.

Isothermal oxidation of coked HZSM-5 zeolite

Two series of isothermal oxidation of the coked HZSM-5 zeolite was conducted by using 2.1% O_2 (air/nitrogen volume ratio = 1/9) as carrier gas at 640℃ and 680℃, respectively. For each series, a completely oxidation run was firstly carried out to acquire the profile of the isothermal oxidation. Then a series of partial isothermal oxidation runs with designed oxidation degrees were conducted by controlling the oxidation time. In a typical run of isothermal oxidation at 640℃ (or 680℃), 150 mg coked HZSM-5 catalyst sample was placed

in a U-shaped quartz tube. The sample was pretreated at 230℃ for 40 min under pure nitrogen. A bypass line was designed for the carrier gas, and flow rate of the carrier gas that passing the coked catalyst sample was generally set to 50 cm^3/min. Then, the temperature was raised to 640℃ (or 680℃) with a ramp rate of 20 ℃/min. As the temperature tended to stabilize at 640℃ (or 680℃), an air stream (pretreated by CO_2 removal and drying) with flow rate of 50 cm^3/min was mixed to the main pipeline of the carrier gas to initiate the oxidation reaction. The contents of H_2O and CO_2 in the outlet gas stream were measured by a dew point transmitter (SF52, Michell Instruments) and an infrared carbon dioxide analyzer (GXH-1050, JUN-FANG-LI-HUA Technology-research Institute Beijing China), respectively. When the operating time of the oxidation reaction reached the preset value, the air stream was switched off (the flowing nitrogen was preserved) and the furnace was open to quench the U-shaped tube in atmosphere immediately. The released volume of the micropores of the series sample prepared by partial isothermal oxidization at 680℃ were measured by nitrogen adsorption-desorption isotherms at -196℃ on a physical adsorption instrument of JW-BK200C (JWGB SCI. & TECH).

Acidity characterization

Based on the mechanism of the decomposition reaction of alkyl amine over Brønsted acid sites[45], the Brønsted acidity of HZSM-5 zeolite was characterized by the temperature-programmed decomposition of *n*-propylamine (*n*-propylamine TPD) method[46] on a self-designed setup[13]. In a typical run, *ca*. 20 mg catalyst sample was first placed in a U-shaped quartz tube and heated up to 550℃ from room temperature (20 ℃/min), and then it was degassed at 550℃ for 1 hour in 30 cm^3/min flowing nitrogen. After cooled down to

175℃, the *n*-propylamine adsorption was conducted by switching the carrier gas to *n*-propylamine saturated (at 0℃) nitrogen gas for 15 min. Thereafter, pure nitrogen was switched back to remove the physically adsorbed *n*-propylamine at 175℃ for 30 min. After passing through a gas-washing cuvette containing H_2SO_4 aqueous solution (1.0 mol/L), which was designed to remove the physically desorbed *n*-propylamine or ammonia produced by *n*-propylamine decomposition under a low temperature condition (provided by ice-water bath for the suppression of the oligomerization of propylene), the gaseous stream flowing out the U-shaped tube was introduced to a flame ionization detector (FID) detector. When the FID signal tended to stabilize, the sample was heated up to 720℃ with a ramp rate of 10 ℃/min, while the content of propylene produced by *n*-propylamine decomposition was recorded by the FID detector simultaneously. The acid density was calculated from the integral area of the *n*-propylamine TPD profiles, which was verified in Figure S1 and Figure S2. While the acid strength was evaluated by taking the maximum temperature or the average temperature of the *n*-propylamine TPD profiles as an apparent index, which was proved to be positively related to the intrinsic acid strength (deprotonation energy, E_{DEP}) of the Brønsted acid sites (Figure S3). The possible influences of diffusion and re-adsorption/desorption on the measurement of acid strength from *n*-propylamine TPD profiles have been exclude (Figure S4).

Following the procedure introduced in our previous work[47], the *n*-dodecane TPSR method (denoted as *n*-C_{12} TPSR) was used to reflect the acidic properties of HZSM-5 zeolite from another perspective. Although it was not possible to distinguish Brønsted acid from Lewis acid, this method was used to evaluate the effective acid sites that can catalyze the probe

reaction of *n*-dodecane cracking semi-quantitatively.

RESULTS AND DISCUSSION

Completely deactivated HZSM-5 prepared by coke deposition

The model reaction of supercritical catalytic cracking of *n*-dodecane at 500℃ under 4.0 MPa with WHSV = 45 h^{-1} was applied to deposit sufficient coke so as to deactivate all the Brønsted acid sites of HZSM-5 zeolite. In Figure 1a, the evolution of the catalytic activity *vs.* time on stream (TOS) clearly demonstrates that completely deactivation of HZSM-5 had been achieved when TOS reached 240 min. According to the temperature-programmed oxidation (TPO) analysis (Figure S5), the coke content and H/C molar ratio of the completely deactivated HZSM-5 (denoted as Coked-HZSM-5) were calculated to be 9.85 ± 0.09 wt.% and 0.38 ± 0.02, respectively.

In order to assess the potential effects of the manipulation of coke deposition and oxidation, the acidic and physical properties of fresh HZSM-5, Coked-HZSM-5 and regenerated HZSM-5 (completely oxidized by isothermal oxidation at 680℃ using 2.1% oxygen) zeolite catalysts were compared. The acidity characterized by *n*-propylamine TPD method was shown in Figure 1b. Obviously, the coke deposition can cause the loss of the majority of the Brønsted acid sites (94.4%) and the shift of the maximum temperature (T_m) towards higher temperature, while the following oxidation can successfully recover most of the acidity (97.8%) as expected. Based on the nitrogen adsorption-desorption analysis (Figure S6), all the micropores of Coked-HZSM-5 have been lost while the majority of the micropores (91%) can be recovered again by oxidation (Table 1). The characteristic variation on the XRD pattern caused by coke deposition also appeared[13], but the crystal structure can be reversibly

recovered by the following oxidation (Figure S7). Thus, the manipulation of coke deposition and oxidation is proved to be an effective strategy to mask and release the Brønsted acid sites without obvious irreversible damage on textural or crystalline properties of HZSM-5 zeolite.

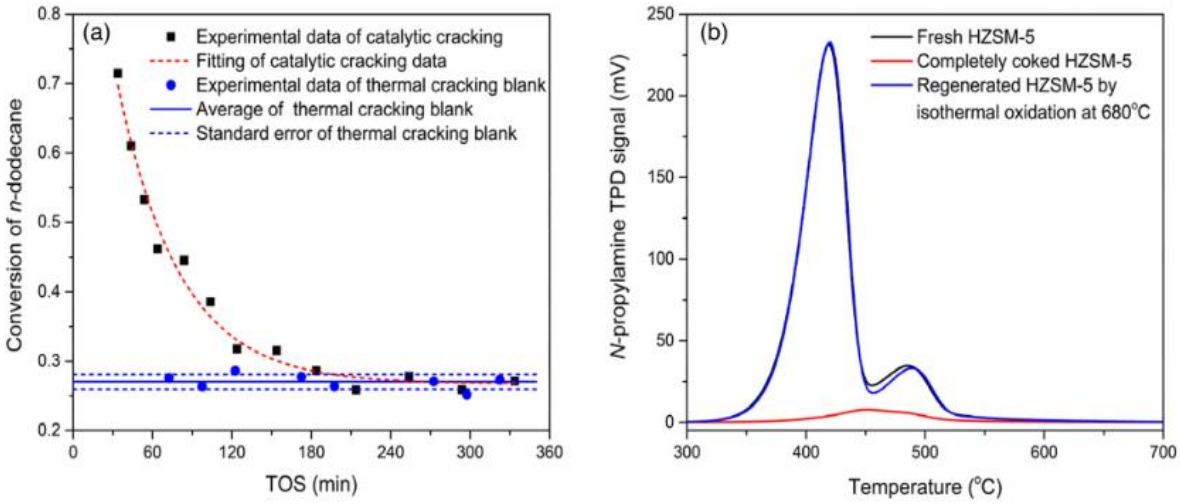

FIGURE 1 Masking and recovery of the acidity of HZSM-5 via coke deposition and oxidation: (a) evolution of the catalytic activity of HZSM-5 zeolite versus TOS in the supercritical catalytic cracking of *n*-dodecane (500°C, 4.0 MPa and WHSV = 45 hr^{-1}); (b) comparison of the acidity of fresh, completely coked and regenerated HZSM-5 by *n*-propylamine TPD method [Color figure can be viewed at wileyonlinelibrary.com]

TABLE 1 The textural properties of fresh HZSM-5, coked-HZSM-5, and regenerated HZSM-5 zeolite catalysts

Samples	S_{Micro}[b] (m^2/g)	$S_{External}$ (m^2/g)	S_{BET} (m^2/g)	V_{Micro}[b] (cm^3/g)	$V_{External}$ (cm^3/g)	V_{Total}[c] (cm^3/g)
Fresh HZSM-5	337.2	23.2	360.4	0.137	0.043	0.180
Coked-HZSM-5	0	11.0	11.0	0	0.055	0.055
Calibrated Coked-HZSM-5[d]	0	12.2	12.2	0	0.061	0.061
Regenerated HZSM-5	304.5	38.7	343.2	0.125	0.068	0.193

[a]Calculated by the t-plot method.
[b]Specific surface area calculated by BET method.
[c]Calculated according to the quantity of N2 adsorbed at P/P0 = 0.99.
[d]The calibration is conducted by converting the basis mass of the coked-HZSM-5 sample from the apparent sample mass (containing both the pure HZSM-5 zeolite and deposited coke) to the pure HZSM-5 zeolite (subtracting the mass of coke from the mass of the coked-HZSM-5 sample).

Combined with the coke content and textural data, the apparent average coke density $\overline{\rho_{cA}}$ was calculated to be 0.828×10^3 kg/m^3 by Equation (1). As a type of complex polycyclic aromatic hydrocarbons[48], the direct measurement of the intrinsic density of the coke deposited in micropores is quite difficult. The value of 1.22×10^3 kg/m^3, as the density of coal with H/C ratio of 0.8, was generally taken as a reference density for internal coke based on the similarity of H/C ratio[49,50]. However, the significant deviation of the H/C ratio of the coke in this work (0.38) from that of coal makes the reference intrinsic coke density (1.22 ×

10^3 kg/m^3) not applicable. Since it is a feasible idea to predict the density of organic materials from the elemental composition[51], the density data of several known polycyclic aromatic hydrocarbons with different H/C ratios has been surveyed based on open database to estimate the intrinsic density of the coke deposited on Coked-HZSM-5 (Table S1). Then, an empirical exponential correlation was made between the intrinsic density and H/C ratio within the range of 0.4 < H/C ratio < 0.80 (Figure S5). Then the intrinsic density of the deposited coke is extrapolated to be 1.73 × 10^3 kg/m^3 according to its H/C ratio, which is approximately twice of the apparent density. This indicates that the coke spatial distribution is nonuniform, *i.e.*, approximate half of the micropores are lost due to the pore blockage rather than site coverage by coke.

$$\overline{\rho_{cA}} = \frac{\frac{c_{coke}}{1-c_{coke}}}{V_{T0}-V_{Tf}} = \frac{\frac{0.0985}{1-0.0985}}{0.193-0.061} = 0.828 \times 10^3 \text{ kg/m}^3 \quad (1)$$

where $\overline{\rho_{cA}}$ is the average apparent coke density of coked-HZSM-5 simply calculated by dividing coke content by the lost pore volume, kg/m^3; c_{coke} is the apparent coke content, wt.%; V_{T0} and V_{Tf} are the total pore volume of regenerated HZSM-5 and Coked-HZSM-5, respectively, cm^3/g.

Since granular HZSM-5 catalyst (20-40 mesh, sub-millimeter size) was used to prepare the Coked-HZSM-5 zeolite, which consists of the massive aggregates of crystal grains, it is necessary to check whether the isothermal oxidation is controlled by intra-crystal or inter-crystal (*i.e.*, intra-particle) process. Therefore, the Coked-HZSM-5 catalyst sample was ground to a small particle size (60-80 mesh), and then the isothermal oxidation profiles of different particle sizes were acquired under the same conditions of isothermal oxidation (Figure S9). Since no obvious difference can be found in Figure S9, the isothermal oxidation

of Coked-HZSM-5 catalyst was not controlled by the intra-particle coke oxidation process. The possible effect of external diffusion on the isothermal oxidation was also excluded by comparison of the isothermal oxidation profiles obtained with different flow rates of carrier gas (Figure S10).

In summary, the manipulation of coke deposition and oxidation is an effective method to mask and release the Brønsted acid sites of HZSM-5 zeolite catalyst on the level of crystal grains without obvious damage of crystal or textural structures. However, the nonuniform coke distribution also brings complexity for the following process modelling.

Quantitative description for coke oxidation process

If the oxidation of the Coked-HZSM-5 conforms to the shrinking unreacted model (SCM), then the acid sites released from the outer surface to the center of the crystal grains can be tracked accordingly. Generally, the typical SCM is based on two assumptions: first, the solid particles have regular geometry (generally assumed to be sphere) and single particle size; second, the spatial distribution of the solid reactant within the whole solid particle is uniform[52]. However, the situation is much more complicate in this work since the commercial HZSM-5 zeolite powder consists of crystal grains with different shapes (nonspherical) and sizes (Figure S11) and the spatial distribution of the coke is also nonuniform as mentioned in section 3.1.

In order to quantitative describe such complicate oxidation process, we proposed an enhanced shrinking core model (ESCM), which is quantitatively described by Equation (2~4). The critical improvements of ESCM compared with the typical SCM are introduced below. Firstly, a one-dimensional *pseudo-position coordinate* (L_p) is defined as the reaction

coordinate on the basis of the CO_2 generation data during the isothermal oxidation of Coked-HZSM-5. From another perspective, dL_p can be regarded as the thickness of coke layer of the surface reaction zoon. Secondly, a volume expansion coefficient (δ_e) is introduced to account for the nonuniform spatial distribution of coke. The main assumption is that the coke deposited within the micropores of HZSM-5 zeolite is discontinuous, the total volume deactivated by a differential element volume of coke is the sum of the exact volume occupied by coke and the adjacent void volume blocked by corresponding coke. Thirdly, the *real-position coordinate* (L_{rp}), defined as the thickness of the oxidized layer (similar to "*ash layer*" in typical SCM) of the nonspherical Coked-HZSM-5 crystal grains (or the shortest distance from the outer surface of crystal grains to the reaction front), can be calculated by the combination of L_p and δ_e. Fourthly, the parameter S_p, defined as the total surface area of the shrinking unreacted core of all the crystal grains contained in the Coked-HZSM-5 sample, can be decoupled from L_p. Then the relationship of V_p (the volume of the released micropores in the oxidized layer)-S_p-L_p can now be deduced from experimental measurement rather than be simulated by the volume formula of an arbitrary geometry. Thus, problem caused by the complexity of non-regular shape (nonspherical) and crystalline grain size distribution of the commercial HZSM-5 zeolite catalyst can be solved. Fifthly, the differential intrinsic coke density (ρ_{cI}) is involved to calculate the exact differential volume occupied by individual coke element from the mass of the coke that has already been oxidized. Additionally, the degree of the oxidation of Coked-HZSM-5 (X_c) can be defined from the solid phase, *i.e.*, the removal of coke deposited on the catalyst (Equation (5)). One the other hand, an approximate expression of X_c (Equation (6)) can also be derived from the generation of the main gaseous phase

product of CO_2. Since the H/C ratio is fairly low, the deviation in the calculation of X_c caused by the variation of the instantaneous H/C ratio during the shrinking core mode oxidation process is limited and negligible.

$$V_p = \int_0^{L_p} \delta_e S_p dL_p \tag{2}$$

$$L_{rp} = \int_0^{L_p} \delta_e dL_p \tag{3}$$

$$\rho_{cI} = \overline{\rho_{cA}} \cdot \rho_{cA} \delta_e \tag{4}$$

$$X_c = \frac{\int_0^{L_p} S_p \rho_{cI} dL_p}{\int_0^{L_p^{\infty}} S_p \rho_{cI} dL_p} \tag{5}$$

$$X_c \approx \frac{\int_0^{t} Y_{CO_2} dt}{\int_0^{t^{\infty}} Y_{CO_2} dt} \tag{6}$$

where ρ_{cA} is the ratio of differential apparent coke density corresponding to the location of L_p; Y_{CO_2} is the volume fraction of CO_2 in the gaseous stream effluent from the U-shaped oxidation reactor, %; and t is the time on stream of the isothermal oxidation of Coked-HZSM-5, s.

Shrinking core mode isothermal oxidation of Coked-HZSM-5

The next issue is to find the appropriate operating conditions, under which the shrinking core mode oxidation of Coked-HZSM-5 can be achieved. Inspired by our previous work on coke characterization[13], we consider that the opportunity that the shrinking core mode oxidation of the coke deposited in porous zeolite catalyst is preferred might arise in the isothermal oxidation under conditions of high temperature and low oxygen concentration. Such idea is based on the following facts. Firstly, the oxidation of the coke deposited in the porous catalyst at low temperature (450°C) was considered to follow homogeneous model rather than SCM[52]. Secondly, the SCM model is applicable when the chemical reaction rate is

very rapid while the diffusion of gases is sufficiently slow[52]. Thirdly, according to the Arrhenius equation, the relative magnitude of the chemical reaction rate *vs*. diffusion rate of the gaseous reactant can be enhanced by raising temperature since the activation energy of chemical reaction is much greater than that of the physical diffusion. Finally, the low oxygen concentration is helpful to narrow the zoon of the reaction front between the unreacted core and oxidized layer[13].

We propose a discriminant criterion for the shrinking core mode oxidation on the basis of comparing the "fingerprints" extracted from tracking the evolution of the released acid sites with increasing oxidation degree under different candidate operating conditions of isothermal oxidation. In order to extract the "fingerprints" comprehensively, the *n*-propylamine TPD and *n*-dodecane TPSR methods were involved to characterize the released Brønsted acidity and effective acidity, respectively. The diversity of the two probe reactions (*n*-propylamine decomposition *vs. n*-dodecane cracking) stems from the differences in both the difficulty of individual probe reactions and the size of individual probe molecules. The *n*-propylamine TPD is certainly occurring at Brønsted acid sites and the requirement for acid strength is limited[45]. While the *n*-C_{12} TPSR requires relatively strong acid strength but not limited to Brønsted acid sites. Additionally, the difference in molecule size of the two probe molecules might also lead to different potential effects of the host framework atoms on the guest probe molecule[53]. The diversity of the above two methods provides the opportunity to extract the "fingerprints" of acid sites released comprehensively.

Isothermal oxidation of Coked-HZSM-5 at 640℃ and 680℃ using 2.1% O_2 as carrier gas were chosen as the candidate operating conditions for the shrinking core mode oxidation.

Theoretically, if the isothermal oxidation carried out under the candidate conditions conforms to SCM, the sequence of acid sites released should be solely determined by the spatial distribution of individual acid sites and should not be affected by the oxidation temperature. In other words, the "fingerprints" of the released acid sites extracted from the two candidate operating conditions should coincide. Else, if agrees with the *homogeneously model*, the sequence of the individual acid sites released by isothermal oxidation should be affected by the operating temperature. Although no definite correlation has been found between the coke nature and the strength of the deactivated acid site[54], the difficulty of the oxidation of the coke is expected to increase with the increasing strength of the acid site covered or blocked. In order to verify this speculation, the coke deposited on a reference catalyst sample of H-[Fe]-MFI, which has definite weaker intrinsic acid strength than H-[Al]-MFI (*i.e.*, general HZSM-5 zeolite)[55], was produced in the same way to the preparation of Coked-HZSM-5 sample. TPO measurements were applied to identify the difficulty in coke oxidation. According to the TPO profiles in Figure S12, the coked H-[Fe]-MFI exhibits significant lower peak maximum (T_m) than that of coked H-[Al]-MFI (515℃ *vs*. 584℃) as expected. The oxidation of the coke with higher T_m in TPO profile should have priority over the coke with T_m if the isothermal oxidation was operated at higher temperature due to the difference in oxidation activation energy, which has been proved by the comparison of the isothermal oxidation of the coked H-[Fe]-MFI and coked H-[Al]-MFI at different temperature shown in Figure S13.

The evolution of the *n*-propylamine TPD profiles with increasing conversion of coke oxidation reaction (denoted as X_c) exhibit similar trends for the isothermal oxidation

conducted at 640℃ and 680℃ in Figure 2a and Figure 2c, *i.e.*, the main Brønsted acid peak temperature decreases with increasing X_c. This preliminary proves that the coke oxidation follows SCM. Although, the distribution of effective acidity is quite different from the distribution of Brønsted acid (Figure 2b *vs*. Figure 2a or Figure 2d *vs*. Figure 2c), the similar evolution of the *n*-C_{12} TPSR profiles with increasing X_c for isothermal oxidation at 640℃ (Figure 2b) and that at 680℃ (Figure 2d) provides additional support for the applicability of SCM from another perspective. The quantitative comparison of the evolution of both acid amount and apparent acid strength (characterized by an index of the average temperature of corresponding profiles) with X_c (Figure S14) clearly confirms that the processes of the acid release during the isothermal oxidation at 640℃ and 680℃ are consistent. Therefore, it can be concluded that the "fingerprints" extracted from the evolution of the released acid sites during the two candidate isothermal oxidation operations (640℃ and 680℃) coincide with each other.

Further, a control experiment was also designed to extract the "fingerprints" of the released acid sites during normal TPO treatment of Coked-HZSM-5 (using air as carrier gas). As shown in Figure S15, the evolution of the properties of the released acid sites characterized by either *n*-propylamine TPD or *n*-C_{12} TPSR profiles exhibits different trends ("fingerprints") to those of the isothermal oxidations shown in Figure 2 and Figure S14. The different "fingerprints" of the released acid sites obtained by normal TPO proves that the matching "fingerprints" of the released acid sites obtained by isothermal oxidation at 640℃ and 680℃ is not accidental but inevitable. Additionally, the faster increase of apparent acid strength of the released acid sites with increasing oxidation degree during the TPO process than that

during the isothermal oxidation process (Figure S15e) confirms that the coke which is difficult to oxidize prefers to deposit on strong acid site.

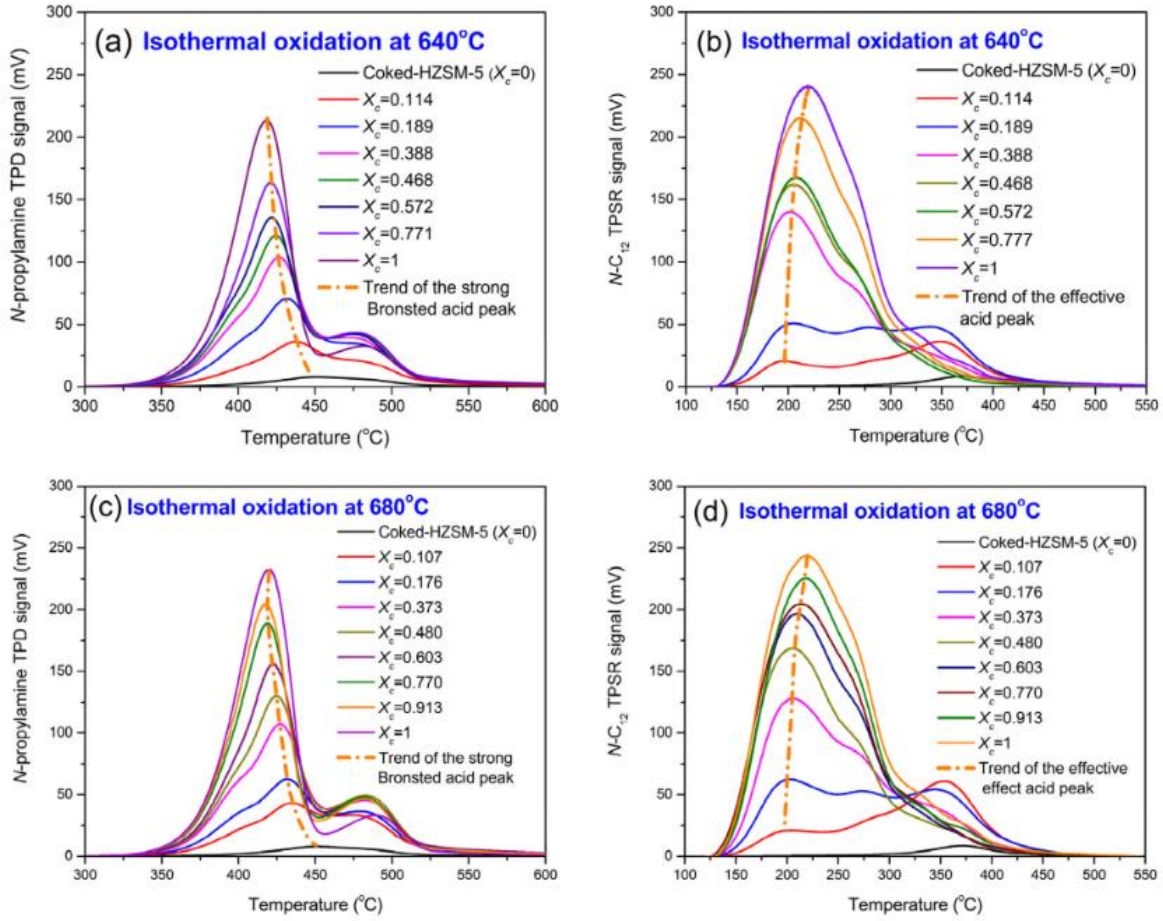

FIGURE 2 Evolution of the released acidity of Coked-HZSM-5 zeolite during isothermal oxidation using 2.1% oxygen (balanced by nitrogen) as carrier gas: (a) *n*-propylamine TPD profiles of isothermal oxidation at 640°C; (b) *n*-C_{12} TPSR profiles of isothermal oxidation at 640°C; (c) *n*-propylamine TPD profiles of isothermal oxidation at 680°C; (d) *n*-C_{12} TPSR profiles of isothermal oxidation at 680°C [Color figure can be viewed at wileyonlinelibrary.com]

In summary, the isothermal oxidation of Coked-HZSM-5 at high temperature (≥ 640°C) and low oxygen concentration (2.1%) conforms shrinking core model and can be used to investigate the spatial distribution of acid sites on the level of crystal grains.

Solution of the enhanced shrinking core model (ESCM)

In order to correlate the released acidity of partially oxidized Coked-HZSM-5 with distinct spatial position on the level of crystal grains, the *real-position coordinate* L_{rp} should be calculated.

The first step is to calculate the *pseudo-position coordinate* L_p by solving the ESCM according to the *in situ* CO_2 generation data monitored during isothermal oxidation at 680℃ using 2.1% oxygen as carrier gas. The details for the calculation of L_p can be found in the supplementary materials and the solution is expressed by Equation (7). Obviously, the spatial scanning on the level of HZSM-5 zeolite crystal grains has been successfully converted to the time scanning of CO_2 generation data during the isothermal oxidation of the coke deposited Coked-HZSM-5 zeolite, the calculation of which is fairly simple. Then, combining the intrinsic coke density correlated from the differential H/C ratio of coke and the V_p measured by nitrogen adsorption-desorption isotherms, the equations of coke spatial distribution (Equation (2) & Equation (3)) can be completely solved.

$$\frac{L_p}{L_p^{\infty}} = \frac{\int_0^t \left(Y_{O_{2,0}} - r_{sp}(1+\delta_{CO_2})Y_{CO_2}\right)dt}{\int_0^{t^{\infty}} \left(Y_{O_{2,0}} - r_{sp}(1+\delta_{CO_2})Y_{CO_2}\right)dt} \tag{7}$$

where $Y_{O_{2,0}}$ is the volume fraction of oxygen at the inlet of the oxidation reactor, r_{sp} is the split ratio of the carrier gas (*e.g.* r_{sp} = 10 when the actual flow rate of carrier gas passing through the catalyst bed is 50 mL/min and the total flow rate of the carrier gas is 500 cm^3/min); δ_{CO_2} is the chemical expansion coefficient of coke oxidation reaction corresponding to CO_2; t is the time on steam of the coke oxidation reaction.

Since L_p was obtained indirectly from the gaseous CO_2 generation data during the isothermal oxidation process rather than from the direct observation from solid crystal grains. The calculation of L_p. might be challenged. For instance, whether the coke was distributed all over the whole crystal grain or was only limited in a local region? The complete loss of micropores of Coked-HZSM-5 in Table 1 proves that at least all the outer surface of Coked-HZSM-5 zeolite particles has been covered or blocked by coke. Then the remaining

adverse situation is that the coke might only deposit in an annular region beneath the external surface of the crystal particles. If so, there should be a sharp rise in the amount of the released acid sites at the last stage of isothermal oxidation process due to the sudden exposure of massive unoccupied micropores beneath the annular coke belt. Obviously, the actual results shown in Figure S14a and Figure S14b are not so. Therefore, L_p can be recognized as the *pseudo-position coordinate* of crystal grains with confidence. The geometric meaning of L_p^{∞} is the pseudo-radius of the minimum inner tangential circle of the crystal particle, while it is related to half of the thickness of the largest HZSM-5 zeolite crystal grain in *b*-axis direction in practice.

In practical calculation of L_p and correlation with other variables, the degree of coke oxidation (X_c) is replaced by X_c' (modified X_c discussed in Supplementary Material). The evolution of L_p/L_p^{∞} with increasing degrees of coke oxidation is shown in Figure 3a. In the initial stage of isothermal oxidation, the increase of L_p is quite slow, while at the last stage L_p increases rapidly. This indicates that most of the coke deposited on the region close to the outer surface of the HZSM-5 zeolite grains. There are two possible reasons: one is the extremely nonuniform distribution of the deposited coke within the crystal grains; the other is the nonuniform nature of the crystal grain size distribution.

According to the nitrogen adsorption-desorption analysis of the series of samples obtained by isothermal partial oxidation at 680℃ using 2.1% oxygen as carrier gas (Figure S18 & Table S2), the evolution of the accessible pore volume (V_p) with increasing degrees of coke oxidation is tracked. In order to verify whether the acid density varies with its spatial distribution, the trend of the evolution of relative V_p *vs*. X_c' is compared with the relative acid

amount characterized by *n*-propylamine TPD during isothermal oxidation at 640℃ and 680℃. It should be noted that both the relative V_p and the relative acid amount have been converted from the "gross-based" original data to the "dry-based" data (*i.e.*, subtract the mass of the residual coke of the partially oxidized sample) for the following calculation. As shown in Figure 3b, the evolution of relative V_p is consistent with the evolution of acidity, demonstrating that the acid density is uniform within the whole crystal grains. Thus, the relative acid amount can also be applied to represent the relative V_p for further calculation. From another point of view, the relationship between V_p and X_c' is nonlinear, indicating that the spatial distribution of the coke is nonuniform.

The differential apparent coke density ($\overline{\rho_{cA}} \cdot \rho_{cA}$) can be used as an index to express the mass-based spatial distribution of coke deposited on Coked-HZSM-5, the physical meaning of which is the mass of coke deposited per unit volume at any position. Through combining Equation (2) and Equation (5), ($\overline{\rho_{cA}} \cdot \rho_{cA}$) can be expressed by Equation (8). The differential intrinsic coke density (ρ_{cI}) can be calculated by combining the differential H/C ratio (Figure S17) and the correlation between intrinsic coke density and H/C ratio (Figure S8). Then the volume expansion coefficient δ_e can be calculated by differential apparent and intrinsic coke density according to the Equation (4). The relationships of the above calculated variables versus X_c' are shown in Figure 3c. The associated positive peak of volume expansion coefficient and negative peak of apparent coke density at X_c = 0.154 can be interpreted as the characteristic of the pore mouth coke.

$$(\overline{\rho_{cA}} \cdot \rho_{cA}) = \frac{dX_c'/dL_p}{dV_p/dL_p} \int_0^{L_p^{\infty}} S_p \rho_{cI} dL_p \tag{8}$$

According to Equation (3), the *real-position coordinate* (L_{rp}) can be calculated by previous

obtained variables of L_p and δ_e. Then spatial distribution of the coke deposited on Coked-HZSM-5 is plotted using the relative L_{rp} (L_{rp}/L_{rp}^{∞}) as the position coordinate (Figure 3d). According to the definition of δ_e, the physical meaning of reciprocal of δ_e ($1/\delta_e$) is the fraction of the volume element that is filled with coke. Thus, $1/\delta_e$ can be taken as the volume-based spatial distribution of coke deposited on Coked-HZSM-5. In Figure 3d, the characteristic peak of pore mouth coke appears at the location of $L_{rp}/L_{rp}^{\infty} = 0.179$. According to the geometric meaning of L_{rp}^{∞} (half of the thickness of the largest crystal grain along the *b*-axis direction), the absolute value of L_{rp}^{∞} is estimated to be *ca*. 356 nm according to SEM image of HZSM-5 zeolite (Figure S11). Then characteristic region of pore mouth coke is approximate 64 nm beneath the outer surface. The analysis about the geometric characteristics of the HZSM-5 zeolite can be found in Figure S19 and corresponding supplementary materials.

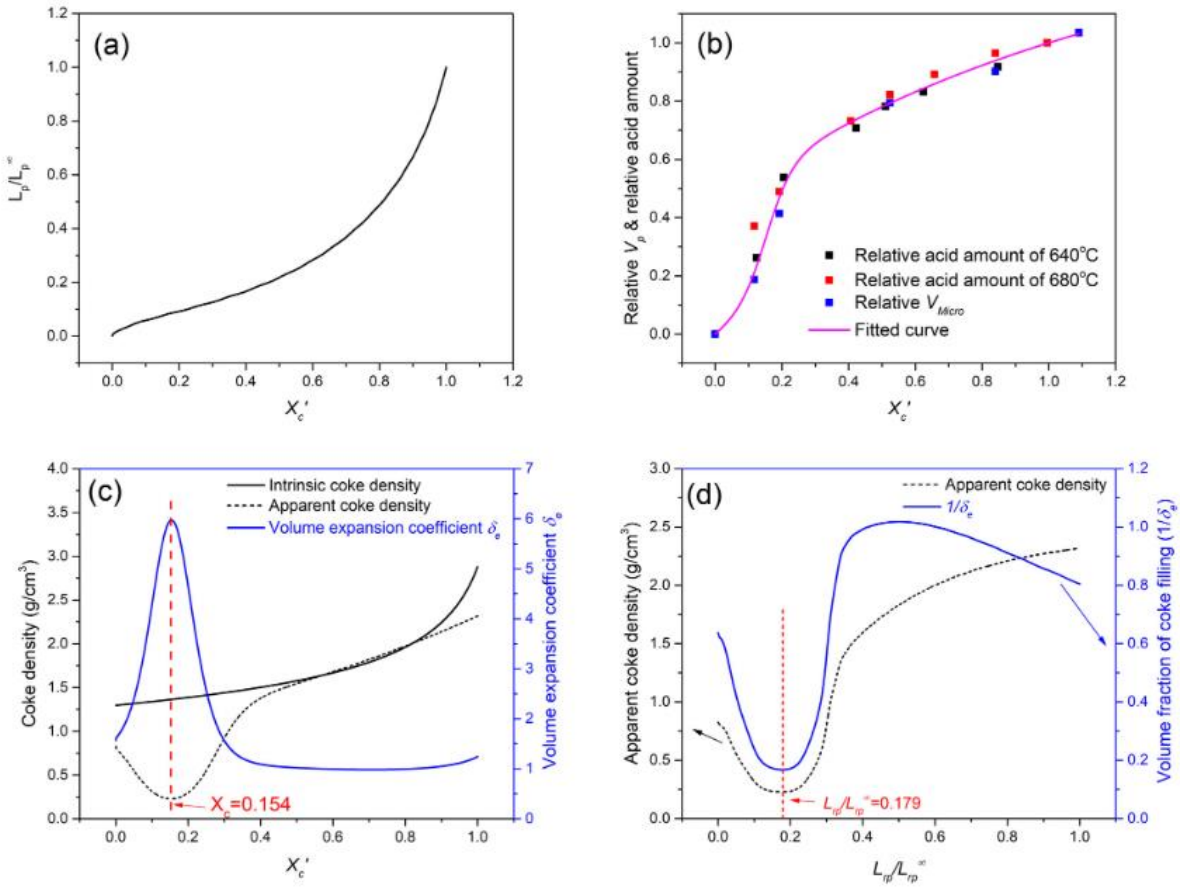

FIGURE 3 The spatial distribution of coke within the crystal grains of Coked-HZSM-5 zeolite: (a) L_p/L_p^{∞} versus X_c'; (b) relative V_p versus X_c'; (c) the coke distribution based on X_c'; (d) the spatial distribution of coke based on L_{rp} [Color figure can be viewed at wileyonlinelibrary.com]

In summary, the ESCM model can be solved successfully by combining the isothermal coke oxidation data (Y_{CO_2} *vs.* *t*), nitrogen adsorption-desorption data (V_p vs. X_c') and intrinsic coke density data (correlated with differential H/C ratio). Then the spatial distribution of coke along with the *real-position coordinate* (L_{rp}) of the HZSM-5 crystal grains with uncertain shapes and a particle size distribution can be constructed according to the solution of ESCM.

Spatial distribution of the Brønsted acid strength

In this section, the spatial distribution of acid strength will be built by combining the *real-position coordinate* (L_{rp}) and the index of apparent Brønsted acid strength characterized by *n*-propylamine TPD method.

Taking the degree of coke oxidation (X_c') as an intermediary, a preliminary correlation of

the acid strength and *real-position coordinate* was obtained based on the data in Figure 3a and Figure S14c. As shown in Figure 4a, a significant difference in the index of apparent acid strength can be observed for the acid sites locating at different position of the HZSM-5 crystal grains. According to the basic theory of *n*-propylamine TPD method, the decrease of temperature means the enhancement of acid strength, thus the acid sites at the center of the crystal grains are stronger than those close to the outer surface. Although the index of apparent acid strength is certainly influenced by the confinement effects[53], the exquisite method design in this work makes it possible to reflect the spatial distribution of the intrinsic acid strength by the index of apparent acid strength (details discussion can be found in Supplementary Material). This results reveal that the acid strength is nonuniform on the level of HZSM-5 crystal grains, which can provide an alternate explanation for the observed difference in the catalytic activity of the Brønsted acid sites at different region of a single HZSM-5 particle according to fluorescence microscope method[40,42-44].

However, the form of the index of apparent acid strength used in Figure 4a is the raw data of cumulative average acid strength of the partially oxidation Coked-HZSM-5 prepared by isothermal oxidation at 680 ℃ rather than the differential acid strength of the individual acid sties. In order to express the acid strength distribution more clearly, the differential acid strength distribution profile can be calculated by Equation (9) and the results are shown in Figure 4b. Obviously, the differential acid strength increases from the outer surface to the center of the crystal grains gradually.

$$E_{AS}(L_{rp}) = \frac{d\left(\left(\frac{F_{AS}(L_{rp})}{F_{AD}(L_{rp})}\right)\cdot F_{AD}(L_{rp})\right)}{E_{AD}(L_{rp})dL_{rp}} = \frac{d\left(\left(\frac{F_{AS}(L_{rp})}{F_{AD}(L_{rp})}\right)\cdot F_{AD}(L_{rp})\right)}{d\left(F_{AD}(L_{rp})\right)} \quad (9)$$

where $E_{AS}(L_{rp})$ and $E_{AD}(L_{rp})$ are the distribution density functions of acid strength and acid

density at the position of L_{rp}, respectively; while $F_{AS}(L_{rp})$ and $F_{AD}(L_{rp})$ are the distribution functions of acid strength and acid density at the position of L_{rp}, respectively; and $\frac{F_{AS}(L_{rp})}{F_{AD}(L_{rp})}$ is the cumulative average acid strength.

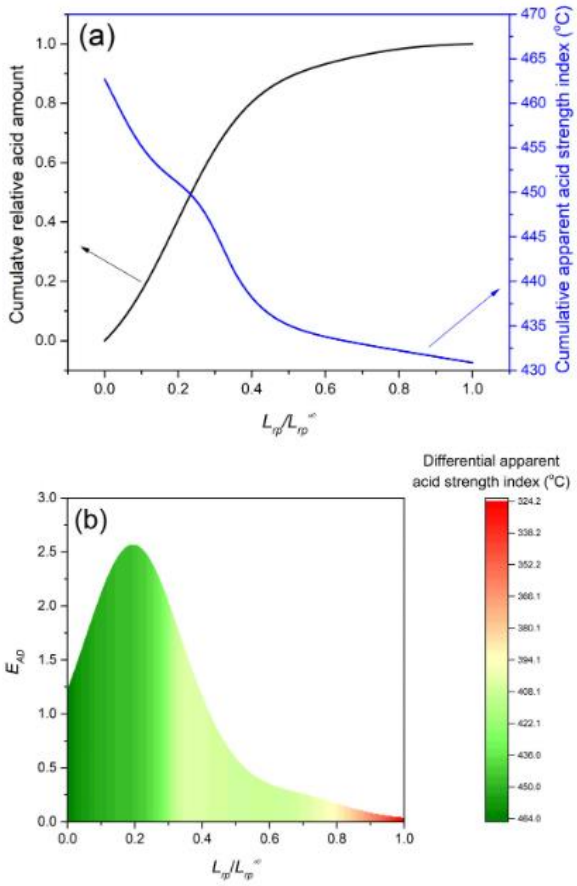

FIGURE 4 The spatial distribution of the Brønsted acidity of the HZSM-5 zeolite on the level of crystal grains: (a) cumulative average acid amount and index of apparent acid strength; (b) differential acid amount and index of apparent acid strength [Color figure can be viewed at wileyonlinelibrary.com]

In summary, the spatial distribution of the acid strength of HZSM-5 zeolite on the level crystal grains can be clearly mapped by the coke manipulating methods proposed in this work. According to this new method, it is revealed that Brønsted acid strength increases from the outer surface to the center of the crystal grains of HZSM-5 zeolite. This work provides an opportunity to explore the unknown long-range interaction of individual acid sites, which is helpful to support the rational design of HZSM-5 zeolite catalyst.

CONCLUSION

Through the combination of the coke manipulation (first deposition by supercritical catalytic cracking of *n*-dodecane and then regeneration by shrinking core mode oxidation) and a bulk acidity characterization method of *n*-propylamine TPD, we developed a feasible method to map the spatial distribution of the Brønsted acidity (acid density and strength) of HZSM-5 zeolite on the level of crystal grains. The shrinking core mode oxidation of the coke deposited on HZSM-5 zeolite is an essential prerequisite to build such new method, which can be achieved by isothermal oxidation under conditions of high temperature (≥ 640°C) and low oxygen concentration (2.1 vol.%). An enhanced shrinking core model (ESCM) was proposed to bridge the gap between the experimental coke oxidation data and the spatial coordinate on the level of crystal grains of HZSM-5 zeolite. By solving the ESCM, the one-dimensional *position coordinate* (L_{rp}), defined as the thickness of the oxidized layer, can be calculated simultaneously with the spatial distribution of coke. Then the Brønsted acidities of a series of HZSM-5 samples prepared by different extent of partial oxidation under shrinking core mode were characterized by *n*-propylamine TPD method. The results reveal that the acid density is uniform on the level of crystal grains while the acid strength rises from the outer surface to the center of HZSM-5 zeolite crystal grains. This method has two significant advantages in studying the acidic properties on the level of crystalline particle: first, the difficult direct spatial scanning of acidity within the crystal grains can be converted to the easy indirect time scanning of coke oxidation under shrinking core mode; second, a feasible, inexpensive bulk method of *n*-propylamine TPD can be used to characterize the spatial distribution of the acidity. According to the mechanism, this method can be extended to map the spatial distribution of coke or acidity of other types of valuable zeolite catalysts.

ACKNOWLEDGMENTS

This work was financially supported by National Natural Science Fund of China (21206201), the Fundamental Research Funds for the Central Universities (CQDXWL-2013-017, 106112017CDJXFLX0014 and 2018CDXYHG0028), the Chongqing Foundation and Advanced Research Projects (cstc2016jcyjA0462) and the Chongqing science and technology project (No. cstc2018jszx-cyzdX0087).

REFERENCES

1. Corma A, Corresa E, Mathieu Y, Sauvanaud L, Al-Bogami S, Al-Ghrami MS, Bourane A. Crude oil to chemicals: light olefins from crude oil. *Catalysis Science & Technology.* 2017;7(1):12-46.

2. Shi J, Wang Y, Yang W, Tang Y, Xie Z. Recent advances of pore system construction in zeolite-catalyzed chemical industry processes. *Chem. Soc. Rev.* 2015;44(24):8877-8903.

3. Yarulina I, De Wispelaere K, Bailleul S, Goetze J, Radersma M, Abou-Hamad E, Vollmer I, Goesten M, Mezari B, Hensen EJM, Martínez-Espín JS, Morten M, Mitchell S, Perez-Ramirez J, Olsbye U, Weckhuysen BM, Van Speybroeck V, Kapteijn F, Gascon J. Structure–performance descriptors and the role of Lewis acidity in the methanol-to-propylene process. *Nature Chemistry.* 2018;10(8):804-812.

4. Bailleul S, Yarulina I, Hoffman AEJ, Dokania A, Abou-Hamad E, Chowdhury AD, Pieters G, Hajek J, De Wispelaere K, Waroquier M, Gascon J, Van Speybroeck V. A Supramolecular View on the Cooperative Role of Bronsted and Lewis Acid Sites in Zeolites for Methanol Conversion. *J. Am. Chem. Soc.* 2019;141(37):14823-14842.

5. Mueller S, Liu Y, Vishnuvarthan M, Sun X, van Veen AC, Haller GL, Sanchez-Sanchez M, Lercher JA. Coke formation and deactivation pathways on H-ZSM-5 in the conversion of methanol to olefins. *J. Catal.* 2015;325:48-59.

6. Liang T, Chen J, Qin Z, Li J, Wang P, Wang S, Wang G, Dong M, Fan W, Wang J. Conversion of Methanol to Olefins over H-ZSM-5 Zeolite: Reaction Pathway Is Related to the Framework Aluminum Siting. *Acs Catalysis.* 2016;6(11):7311-7325.

7. Losch P, Pinar AB, Willinger MG, Soukup K, Chavan S, Vincent B, Pale P, Louis B. H-ZSM-5 zeolite model crystals: Structure-diffusion-activity relationship in methanol-to-olefins catalysis. *J. Catal.* 2017;345:11-23.

8. Chowdhury AD, Paioni AL, Houben K, Whiting GT, Baldus M, Weckhuysen BM. Bridging the Gap between the Direct and Hydrocarbon Pool Mechanisms of the Methanol-to-Hydrocarbons Process. *Angewandte Chemie-International Edition.* 2018;57(27):8095-8099.

9. Wu X, Xu S, Zhang W, Huang J, Li J, Yu B, Wei Y, Liu Z. Direct Mechanism of the First Carbon-Carbon Bond Formation in the Methanol-to-Hydrocarbons Process. *Angewandte Chemie-International Edition.* 2017;56(31):9039-9043.

10. Liu Y, Mueller S, Berger D, Jelic J, Reuter K, Tonigold M, Sanchez-Sanchez M, Lercher JA. Formation Mechanism of the First Carbon-Carbon Bond and the First Olefin in the Methanol Conversion into Hydrocarbons. *Angewandte Chemie-International Edition.* 2016;55(19):5723-5726.

11. Sadrameli SM. Thermal/catalytic cracking of liquid hydrocarbons for the production of olefins: A state-of-the-art review II: Catalytic cracking review. *Fuel.*

2016;173:285-297.

12. Mohammadparast F, Halladj R, Askari S. The Crystal Size Effect of Nano-Sized ZSM-5 in the Catalytic Performance of Petrochemical Processes: A Review. *Chem. Eng. Commun.* 2015;202(4):542-556.

13. Xian X, Ran C, Nai C, Yang P, Zhao S, Dong L. Characterization of the location of coke deposited on spent HZSM-5 zeolite by special temperature-programmed oxidation and isothermal oxidation methods. *Applied Catalysis a-General.* 2017;547:37-51.

14. Xian X, Liu G, Zhang X, Wang L, Mi Z. Catalytic cracking of n-dodecane over HZSM-5 zeolite under supercritical conditions: Experiments and kinetics. *Chem. Eng. Sci.* 2010;65(20):5588-5604.

15. Xu S, Zhang X, Cheng D-g, Chen F, Ren X. Effect of hierarchical ZSM-5 zeolite crystal size on diffusion and catalytic performance of n-heptane cracking. *Frontiers of Chemical Science and Engineering.* 2018;12(4):780-789.

16. Derouane EG, Védrine JC, Pinto RR, Borges PM, Costa L, Lemos MANDA, Lemos F, Ribeiro FR. The Acidity of Zeolites: Concepts, Measurements and Relation to Catalysis: A Review on Experimental and Theoretical Methods for the Study of Zeolite Acidity. *CarRv.* 2013;55(4):454-515.

17. Knott BC, Nimlos CT, Robichaud DJ, Nimlos MR, Kim S, Gounder R. Consideration of the Aluminum Distribution in Zeolites in Theoretical and Experimental Catalysis Research. *Acs Catalysis.* 2018;8(2):770-784.

18. Sklenak S, Dědeček J, Li C, Wichterlová B, Gábová V, Sierka M, Sauer J. Aluminum

Siting in Silicon-Rich Zeolite Frameworks: A Combined High-Resolution 27Al NMR Spectroscopy and Quantum Mechanics / Molecular Mechanics Study of ZSM-5. *Angew. Chem. Int. Ed.* 2007;46(38):7286-7289.

19. Dědeček J, Sobalík Z, Wichterlová B. Siting and Distribution of Framework Aluminium Atoms in Silicon-Rich Zeolites and Impact on Catalysis. *CarRv.* 2012;54(2):135-223.

20. Dedecek J, Tabor E, Sklenak S. Tuning the Aluminum Distribution in Zeolites to Increase their Performance in Acid-Catalyzed Reactions. *Chemsuschem.* 2019;12(3):556-576.

21. Wang S, Wang P, Qin Z, Chen Y, Dong M, Li J, Zhang K, Liu P, Wang J, Fang W. Relation of Catalytic Performance to the Aluminum Siting of Acidic Zeolites in the Conversion of Methanol to Olefins, Viewed via a Comparison between ZSM-5 and ZSM-11. *Acs Catalysis.* 2018;8(6):5485-5505.

22. Inagaki S, Shinoda S, Kaneko Y, Takechi K, Komatsu R, Tsuboi Y, Yamazaki H, Kondo JN, Kubota Y. Facile Fabrication of ZSM-5 Zeolite Catalyst with High Durability to Coke Formation during Catalytic Cracking of Paraffins. *Acs Catalysis.* 2013;3(1):74-78.

23. Liu H, Wang H, Xing A-H, Cheng J-H. Effect of Al Distribution in MFI Framework Channels on the Catalytic Performance of Ethane and Ethylene Aromatization. *Journal of Physical Chemistry C.* 2019;123(25):15637-15647.

24. Losch P, Boltz M, Bernardon C, Louis B, Palčić A, Valtchev V. Impact of external surface passivation of nano-ZSM-5 zeolites in the methanol-to-olefins reaction.

Applied Catalysis A: General. 2016;509(Supplement C):30-37.

25. Choi M, Na K, Kim J, Sakamoto Y, Terasaki O, Ryoo R. Stable single-unit-cell nanosheets of zeolite MFI as active and long-lived catalysts. *Nature.* 2009;461(7261):246-U120.

26. Sklenak S, Dedecek J, Li C, Wichterlova B, Gabova V, Sierka M, Sauer J. Aluminium siting in the ZSM-5 framework by combination of high resolution 27Al NMR and DFT/MM calculations. *PCCP.* 2009;11(8):1237-1247.

27. Vjunov A, Fulton JL, Huthwelker T, Pin S, Mei D, Schenter GK, Govind N, Camaioni DM, Hu JZ, Lercher JA. Quantitatively Probing the Al Distribution in Zeolites. *J. Am. Chem. Soc.* 2014;136(23):8296-8306.

28. Yokoi T, Mochizuki H, Namba S, Kondo JN, Tatsumi T. Control of the Al Distribution in the Framework of ZSM-5 Zeolite and Its Evaluation by Solid-State NMR Technique and Catalytic Properties. *The Journal of Physical Chemistry C.* 2015;119(27):15303-15315.

29. Yokoi T, Mochizuki H, Biligetu T, Wang Y, Tatsumi T. Unique Al Distribution in the MFI Framework and Its Impact on Catalytic Properties. *Chem. Lett.* 2017;46(6):798-800.

30. Biligetu T, Wang Y, Nishitoba T, Otomo R, Park S, Mochizuki H, Rondo JN, Tatsumi T, Yokoi T. Al distribution and catalytic performance of ZSM-5 zeolites synthesized with various alcohols. *J. Catal.* 2017;353:1-10.

31. Dedecek J, Kaucky D, Wichterlova B, Gonsiorova O. Co2+ ions as probes of Al distribution in the framework of zeolites. ZSM-5 study. *PCCP.* 2002;4(21):5406-5413.

32. Janda A, Bell AT. Effects of Si/Al Ratio on the Distribution of Framework Al and on the Rates of Alkane Monomolecular Cracking and Dehydrogenation in H-MFI. *J. Am. Chem. Soc.* 2013;135(51):19193-19207.

33. Song C, Chu Y, Wang M, Shi H, Zhao L, Guo X, Yang W, Shen J, Xue N, Peng L, Ding W. Cooperativity of adjacent Brønsted acid sites in MFI zeolite channel leads to enhanced polarization and cracking of alkanes. *J. Catal.* 2017;349:163-174.

34. Yang C-T, Janda A, Bell AT, Lin L-C. Atomistic Investigations of the Effects of Si/Al Ratio and Al Distribution on the Adsorption Selectivity of n-Alkanes in Bronsted-Acid Zeolites. *Journal of Physical Chemistry C.* 2018;122(17):9397-9410.

35. Zeets M, Resasco DE, Wang B. Enhanced chemical activity and wettability at adjacent Bronsted acid sites in HZSM-5. *Catal. Today.* 2018;312:44-50.

36. Baba T, Inoue Y, Ono Y. Long-Range Interaction of Alkali Cations with the Acidic OHGroups in H-ZSM-5. *J. Catal.* 1996;159(1):230-235.

37. Baba T, Ono Y. Dynamic properties of protons in solid acids as studied by variable temperature 1H MAS NMR. *Applied Catalysis A: General.* 1999;181(2):227-238.

38. Roeffaers MBJ, Sels BF, Uji-i H, De Schryver FC, Jacobs PA, De Vos DE, Hofkens J. Spatially resolved observation of crystal-face-dependent catalysis by single turnover counting. *Nature.* 2006;439(7076):572-575.

39. Buurmans ILC, Ruiz-Martinez J, Knowles WV, van der Beek D, Bergwerff JA, Vogt ETC, Weckhuysen BM. Catalytic activity in individual cracking catalyst particles imaged throughout different life stages by selective staining. *Nature Chemistry.* 2011;3(11):862-867.

40. Roeffaers MBJ, De Cremer G, Libeert J, Ameloot R, Dedecker P, Bons A-J, Bückins M, Martens JA, Sels BF, De Vos DE, Hofkens J. Super-Resolution Reactivity Mapping of Nanostructured Catalyst Particles. *Angew. Chem.* 2009;121(49):9449-9453.

41. Ristanovic Z, Kerssens MM, Kubarev AV, Hendriks FC, Dedecker P, Hofkens J, Roeffaers MBJ, Weckhuysen BM. High-Resolution Single-Molecule Fluorescence Imaging of Zeolite Aggregates within Real-Life Fluid Catalytic Cracking Particles. *Angewandte Chemie-International Edition.* 2015;54(6):1836-1840.

42. Ristanovic Z, Kubarev AV, Hofkens J, Roeffaers MBJ, Weckhuysen BM. Single Molecule Nanospectroscopy Visualizes Proton-Transfer Processes within a Zeolite Crystal. *J. Am. Chem. Soc.* 2016;138(41):13586-13596.

43. Hendriks FC, Mohammadian S, Ristanovic Z, Kalirai S, Meirer F, Vogt ETC, Bruijnincx PCA, Gerritsen HC, Weckhuysen BM. Integrated Transmission Electron and Single-Molecule Fluorescence Microscopy Correlates Reactivity with Ultrastructure in a Single Catalyst Particle. *Angewandte Chemie-International Edition.* 2018;57(1):257-261.

44. Kumar N, Kalirai S, Wain AJ, Weckhuysen BM. Nanoscale Chemical Imaging of a Single Catalyst Particle with Tip-Enhanced Fluorescence Microscopy. *Chemcatchem.* 2019;11(1):417-423.

45. Kresnawahjuesa O, Gorte RJ, de Oliveira D, Lau LY. A Simple, Inexpensive, and Reliable Method for Measuring Brønsted-Acid Site Densities in Solid Acids. *Catal. Lett.* 2002;82(3):155-160.

46. Bates SA, Delgass WN, Ribeiro FH, Miller JT, Gounder R. Methods for NH3 titration of Brønsted acid sites in Cu-zeolites that catalyze the selective catalytic reduction of NOx with NH3. *J. Catal.* 2014;312:26-36.

47. Xian X, Ran C, Yang P, Chu Y, Zhao S, Dong L. Effect of acidity of HZSM-5/MCM-41 hierarchical zeolite on its catalytic performance in supercritical catalytic cracking of n-dodecane: Experiments and mechanism. *Catalysis Science & Technology.* 2018.

48. Guisnet M, Magnoux P. Organic chemistry of coke formation. *Applied Catalysis A: General.* 2001;212(1–2):83-96.

49. Wan Z, Li GK, Wang C, Yang H, Zhang D. Relating coke formation and characteristics to deactivation of ZSM-5 zeolite in methanol to gasoline conversion. *Applied Catalysis A: General.* 2018;549:141-151.

50. Kim J, Choi M, Ryoo R. Effect of mesoporosity against the deactivation of MFI zeolite catalyst during the methanol-to-hydrocarbon conversion process. *J. Catal.* 2010;269(1):219-228.

51. Kuwata M, Zorn SR, Martin ST. Using Elemental Ratios to Predict the Density of Organic Material Composed of Carbon, Hydrogen, and Oxygen. *Environ. Sci. Technol.* 2012;46(2):787-794.

52. Ishida M, Wen CY. Comparison of kinetic and diffusional models for solid-gas reactions. *AlChE J.* 1968;14(2):311-317.

53. Boronat M, Corma A. What Is Measured When Measuring Acidity in Zeolites with Probe Molecules? *ACS Catalysis.* 2019;9(2):1539-1548.

54. Sahoo SK, Viswanadham N, Ray N, Gupta JK, Singh ID. Studies on acidity, activity and coke deactivation of ZSM-5 during n-heptane aromatization. *Applied Catalysis A: General.* 2001;205(1):1-10.

55. Jones AJ, Carr RT, Zones SI, Iglesia E. Acid strength and solvation in catalysis by MFI zeolites and effects of the identity, concentration and location of framework heteroatoms. *J. Catal.* 2014;312:58-68.